



**HAL**  
open science

## **Ab initio proposition of novel BCN3 hard material based on the intergrowth of wurtzite and pyrite-like motifs**

Samir F. Matar, Michel Nakhl, Mirvat Zakhour, Charbel Kfoury, Adel F. Al Alam, Naïm Ouaini

### ► **To cite this version:**

Samir F. Matar, Michel Nakhl, Mirvat Zakhour, Charbel Kfoury, Adel F. Al Alam, et al.. Ab initio proposition of novel BCN3 hard material based on the intergrowth of wurtzite and pyrite-like motifs. Computational Condensed Matter, 2016, 7, pp.14-19. 10.1016/j.cocom.2016.03.003 . hal-01331775

**HAL Id: hal-01331775**

**<https://hal.science/hal-01331775>**

Submitted on 18 Jan 2021

**HAL** is a multi-disciplinary open access archive for the deposit and dissemination of scientific research documents, whether they are published or not. The documents may come from teaching and research institutions in France or abroad, or from public or private research centers.

L'archive ouverte pluridisciplinaire **HAL**, est destinée au dépôt et à la diffusion de documents scientifiques de niveau recherche, publiés ou non, émanant des établissements d'enseignement et de recherche français ou étrangers, des laboratoires publics ou privés.



## Regular article

Ab initio proposition of novel BCN<sub>3</sub> hard material based on the intergrowth of wurtzite and pyrite-like motifs

Samir F. Matar<sup>a, b, d, \*</sup>, Michel Nakhl<sup>b</sup>, Mirvat Zakhour<sup>b</sup>, Charbel Kfoury<sup>c</sup>, Adel F. Al Alam<sup>d</sup>, Naïm Ouaini<sup>d</sup>

<sup>a</sup> CNRS-ICMCB, Université de Bordeaux, 33600 Pessac, France

<sup>b</sup> Université Libanaise, Faculté des Sciences II, Plateforme de Recherche en Nanotechnologies et Nanomatériaux, Fanar, Lebanon

<sup>c</sup> Université Libanaise, Faculté de Génie, Roumieh, Lebanon

<sup>d</sup> Université Saint Esprit de Kaslik, USEK, Jounieh, Lebanon

## ARTICLE INFO

## Article history:

Received 10 February 2016

Received in revised form

22 March 2016

Accepted 22 March 2016

Available online 12 April 2016

## Keywords:

Hard materials

DFT

High bulk modulus

Brittleness

Insulator

## ABSTRACT

A novel hard material, orthorhombic BCN<sub>3</sub> based on the intergrowth of non-centrosymmetric wurtzite CN<sup>+</sup> and centrosymmetric pyrite BN<sub>2</sub> motifs alike in fully characterized AlSiP<sub>3</sub> ternary is proposed from calculations within DFT methodology. BCN<sub>3</sub> is identified as a “nitride-dinitride” related with Zintl phases. The ground state structure exhibits significantly short interatomic distances: d(C–N) = 1.47 Å and d(N–N) = 1.43 Å as compared to d(Si–P) = 2.24 Å and d(P–P) = 2.18 Å in the phosphide, resulting into high magnitude bulk modulus obtained from E,V equation of state (EOS) with B<sub>0</sub> = 371 GPa versus B<sub>0</sub> = 97 GPa in the phosphide. The complete set of elastic constants complies with the mechanical stability conditions of the new system and equally produces high hardness magnitude (384 GPa). Ratio of bulk/shear modulus of 0.85 characterizes a brittle material. Electronic band structures identify small indirect gap semi-conducting AlSiP<sub>3</sub> and large band gap insulator BCN<sub>3</sub> with direct gap  $T_V-T_C \sim 4$  eV.

© 2016 The Authors. Published by Elsevier B.V. This is an open access article under the CC BY-NC-ND license (<http://creativecommons.org/licenses/by-nc-nd/4.0/>).

## 1. Introduction

Carbon is known in two main forms, two dimensional (2D) in soft graphite and three dimensional (3D) in ultra-hard diamond: cubic (major phase) and hexagonal (*Lonsdaleite*; minor phase). Such an exceptional hardness is the result of strong covalent short carbon-carbon bonds and their isotropic spatial distribution in  $sp^3$  hybridization of carbon *s* and *p* orbitals forming a tetrahedron while it is planar  $sp^2$  hybridization in graphite. Industrial diamond was made available as early as the 1950s by use of high pressure –high temperature techniques [1]. Beside its high cost a problem is raised by the application of artificial diamond in tooling machines, especially when it is used in cutting steel. Such an issue is due to the chemical reactivity of carbon versus metals or alloys at high temperatures caused by the friction, eventually leading to the loss of the quality of diamond (graphitization and combustion) and change of carbon content of steel as well as of the tool. Due to the technological importance underlying the

possibility of discovering novel classes of hard materials, large research efforts have been directed during the last decades towards the synthesis and characterization of promising candidate compounds such as binary boron nitride which is an artificial imitation of carbon. Cubic boron nitride discovered by Bundy and Wentorf is a good substitute for diamond with a hardness magnitude just below 10 which stands for the value assigned to diamond on the Moh scale of hardness with a bulk modulus close de 500 GPa [2]. This property is in part because, unlike diamond, BN does not dissolve into iron, nickel, and related alloys at high temperatures. Due to this electronic similarity, BN adopts similar atomic arrangements as in carbon: three-dimensional (3D) diamond with the cubic *blende* or the hexagonal *wurtzite* structure as well as two-dimensional (2D) graphite (*h*-BN). Also the carbon nitrides C<sub>3</sub>N<sub>4</sub> [3,4] and carbon rich C<sub>11</sub>N<sub>4</sub> [5] were theoretically devised as ultra-hard materials based on Hohenberg, Kohn and Sham quantum density functional theory (DFT) [6] and many subsequent efforts were paid for their syntheses. Besides the above binary systems tetraboron carbide B<sub>4</sub>C is among the hardest materials; its properties were comprehensively reviewed by Thévenot [7]. Within the B – C – N diagram, ultra-hard ternaries obeying these conditions as bonding rules for selective atom pairs such as BC<sub>2</sub>N were theoretically devised [8] and

\* Corresponding author. CNRS-ICMCB, Université de Bordeaux, 33600 Pessac, France.

E-mail address: [Samir.Matar@icmcb.cnrs.fr](mailto:Samir.Matar@icmcb.cnrs.fr) (S.F. Matar).

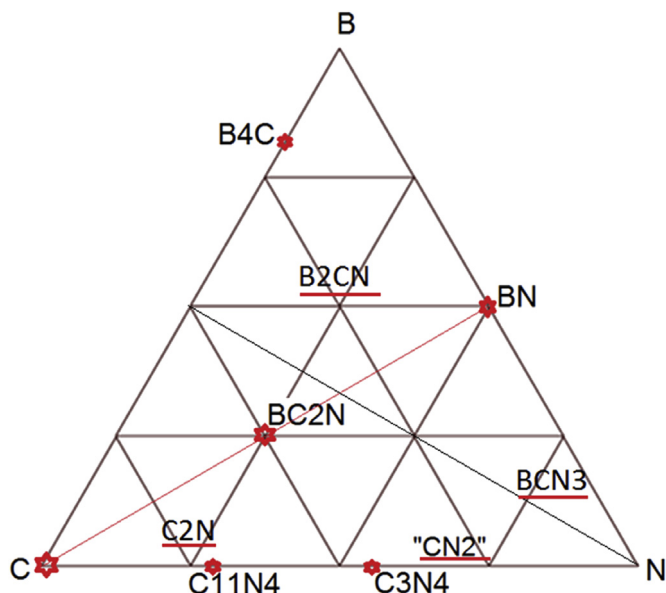


**Fig. 1.** Sketch of the BCN ternary diagram with compositions identified both theoretically and experimentally in the literature. Compounds designated by red stars are isoelectronic with carbon; those non isoelectronic with C are underlined as the model  $\text{BCN}_3$  proposed in this paper.

simultaneously [9] prepared. Most of these compositions follow the isoelectronic rule with carbon (Fig. 1; compositions designated with red stars), i.e. electronically analogue, with:

$$p \cdot Z_V(B) + m \cdot Z_V(C) + l \cdot Z_V(N) = 4 \cdot n$$

where  $p$ ,  $m$ ,  $l$  and  $n$  are integers and  $Z_V(B)$ ,  $Z_V(C)$  and  $Z_V(N)$  correspond to the electron count of the atomic valence states for the three light elements. The underlying idea was that substances satisfying this rule should likely show the same interesting properties of diamond. However some other stoichiometries not obeying this rule were equally proposed as hard materials from first-principles:  $\text{B}_2\text{CN}$  [10] and most recently identified  $\text{C}_3\text{N}$  [11] (Fig. 1; compositions underlined in red).

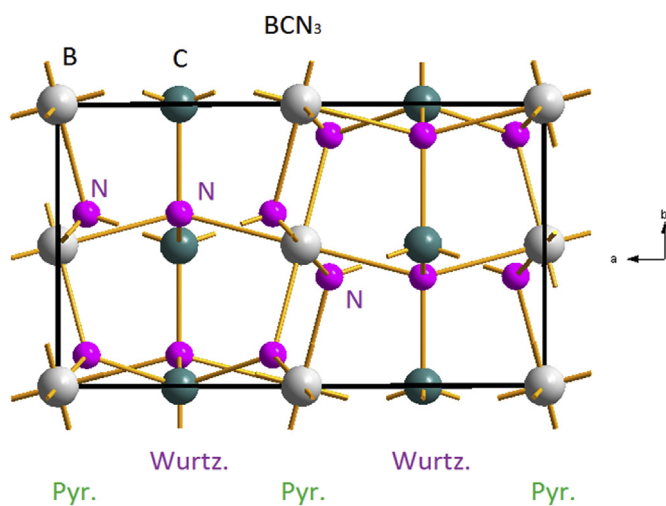


**Fig. 2.**  $\text{BCN}_3$  structure refined from geometry optimization projected onto the  $xOy$  plane ( $a,b$ ) and highlighted as the original and little encountered monoatomic intergrowth of octahedral pyrite " $\text{BN}_2$ " and tetrahedral wurtzite " $\text{CN}^+$ "-like motifs (cf. Fig. 4).

In fact all the stoichiometries within the BCN triangle comply with the requirements for particular mechanical properties as the strength of the bonding which involves short interatomic distances and hence light elements, and the spatial arrangements of atoms and atomic motifs at the microscopic scale.

The ternary compound  $\text{AlSiP}_3$  was prepared and characterized by von Schneering et al. [12] and described as an intergrowth of tetrahedral wurtzite motifs and octahedral pyrite-like ones. The wurtzite planes include  $\text{Si}^{4+}$  cations whereas  $\text{Al}^{3+}$  is at the pyrite plane positions and the structure was described as a succession of  $(\text{SiP})^+ \dots (\text{AlP}_2)^- \dots (\text{SiP})^+ \dots$  etc. (cf. Fig. 2, Table 1). The presence of larger Al in octahedral coordination and Si in tetrahedral coordination is somehow surprising in as far as Si is usually found in octahedral coordination as in  $\text{SiP}_2$  with pyrite structure [13]. However the authors confirmed the retained structural hypothesis against inverting Al and Si positions by lattice energy Madelung calculations.

Based on the above criteria and on the original structure of ternary  $\text{AlSiP}_3$ , a novel hard material  $\text{BCN}_3$  is here proposed using *ab initio* investigations of geometry optimizations and total energy calculations within DFT.

## 2. Computational methodology

Within density functional theory (DFT) framework we used the Vienna *ab initio* simulation package (VASP) code [14,15] which allows geometry optimization and total energy calculations. Subsequent establishment of the energy-volume equations of states EOS, the set of elastic constants and electronic band structure can then be done. The projector augmented wave (PAW) method [15,16], is used with atomic potentials built within the generalized gradient approximation (GGA) scheme following Perdew, Burke and Ernzerhof (PBE) [17]. The conjugate-gradient algorithm [18] is used in this computational scheme to relax the atoms of the different crystal setups. The tetrahedron method with Blöchl corrections [19] as well as a Methfessel-Paxton [20] scheme was applied for both geometry relaxation and total energy calculations. Brillouin-zone (BZ) integrals were approximated using the special k-point sampling of Monkhorst and Pack [21]. The optimization of the structural parameters was performed until the forces on the atoms were less than  $0.02 \text{ eV}/\text{\AA}$  and all stress components less than  $0.003 \text{ eV}/\text{\AA}^3$ . The calculations are converged at an energy cut-off of  $350 \text{ eV}$  for the plane-wave basis set with respect to the k-point integration with a starting mesh of  $6 \times 6 \times 6$  up to  $12 \times 12 \times 12$  for best convergence and relaxation to zero strains.

**Table 1**

Basic crystallographic data for  $\text{AlSiP}_3$  and model  $\text{BCN}_3$  in orthorhombic space group  $Pmnb$  (#62). Al (B) at  $4a$  (0,0,0).

	$\text{AlSiP}_3$ (exp.) [12]	$\text{AlSiP}_3$ (calc.)	$\text{BCN}_3$
<b>Lattice parameters</b>			
$a$ (Å)	9.872	9.873	6.663
$b$ (Å)	5.861	5.873	3.894
$c$ (Å)	6.088	6.102	4.276
$V$ (Å <sup>3</sup> )	352.25	353.80	121.8
<b>Atomic positions</b>			
Si (4c)	$\frac{1}{4}, 0.4992, 0.0616$	$\frac{1}{4}, 0.499, 0.062$	(C) $\frac{1}{4}, 0.506, 0.074$
P1(4c)	$\frac{1}{4}, 0.3876, 0.4139$	$\frac{1}{4}, 0.390, 0.415$	(N1) $\frac{1}{4}, 0.390, 0.419$
P2(8c)	0.0586, 0.389, 0.892	0.058, 0.389, 0.892	(N2) 0.067, 0.39, 0.919
<b>Shortest interatomic distances (Å)</b>			
Al-P2	2.43	2.45	d(B-N2) = 1.61
Si-P1	2.23	2.25	d(C-N1) = 1.46
P2-P2	2.16	2.18	d(N2-N2) = 1.43

### 3. Geometry optimization, energy-volume equation of state EOS, elastic constants and phonons

#### 3.1. Geometry optimization

Firstly we characterize the hitherto unexplored energy derived properties (mainly the bulk module) of  $\text{AlSiP}_3$  [12] by fully relaxing the structure with increasing integration mesh of the reciprocal lattice for best energy and charge convergence. Table 1 provides the experimental and calculated structural parameters showing a good agreement for  $a$ ,  $b$  and  $c$  orthorhombic parameters (and resulting volume) as well as for the atomic coordinates. The interatomic distances are also in agreement with experiment. In the context of the Al octahedral environment with P versus the tetrahedral Si environment with N, we confronted this configuration energetically with the opposite one by exchanging Al and Si positions. The result is a raise of total energy by 0.824 eV per formula unit (FU), leading to confirm the hypothesis retained by the authors of the experimental investigations [12].

Then we turned to the study of  $\text{BCN}_3$  by replacing Al by B, Si by C and P by N so that  $\text{BCN}_3$  is isoelectronic with  $\text{AlSiP}_3$ . The fully relaxed structure after several runs at increasing  $\mathbf{k}$  mesh integration led to retain the orthorhombic structure of  $\text{AlSiP}_3$  in its  $Pmnb$  space group and to systematically smaller lattice parameters, volume and interatomic distances which decrease with similar trends to  $\text{AlSiP}_3$  (Table 1). Clearly upon going from elements of the 2nd period to light and small elements of the 1st large changes are induced which should be noticeable in the mechanical properties (*vide infra*). Lastly for the sake of completeness we tested the effect of exchanging the atomic positions of B and C: The calculations led to equally a raise of the energy by 0.779 eV/FU. Consequently  $\text{BCN}_3$  is proposed in an original hitherto unexplored structure consisting of monoatomic wurtzite-like planes including C and pyrite-like planes with B, leading to the sequence:  $(\text{CN})^+ \dots (\text{BN}_2)^- \dots (\text{CN})^+ \dots (\text{BN}_2)^- \dots$  (cf. Fig. 2). The charge equilibrium is ensured formally in the following manner:  $\text{B}^{3+} \text{C}^{4+} \text{N}^{3-}$  and  $\text{N}_2^{4-}$ , i.e. it is a « nitride-nitride » belonging to Zintl phases as NaTl [22,23].

In this context it was relevant to determine the stability of such stoichiometry firstly by obtaining the cohesive energy  $E_{\text{coh}}$ , on the one hand and confront it with that of  $\text{AlSiP}_3$  on the other hand. Then we examined the mechanical stability from the calculation of the set of elastic constants  $C_{ij}$  (next section).

The cohesive energy is determined from the difference between the compound total electronic energy and those of the atomic constituents. We find:  $E_{\text{coh}}(\text{BCN}_3) = -0.81$  eV/FU versus  $E_{\text{coh}}(\text{AlSiP}_3) = -0.27$  eV/FU. Both compounds are cohesive with negative energies. Also  $E_{\text{coh}}(\text{BCN}_3)$  is three times larger than  $E_{\text{coh}}(\text{AlSiP}_3)$ . This can be explained by the short interatomic distances in  $\text{BCN}_3$  leading to stronger bonding.

#### 3.2. Energy-volume equation of state EOS

For both compounds the agreement with starting experimental data for  $\text{AlSiP}_3$  and the trends obtained for predicted  $\text{BCN}_3$  are good enough to examine the physical properties such as the mechanical ones as the bulk modulus from derived from the energy-volume equation of state (EOS) as well as from the complete set of elastic constants  $C_{ij}$ .

The bulk modulus,  $B(V)$  defines the resistance of the material with respect to elastic and isotropic compression. It is related to the curvature of  $E(V)$ ,

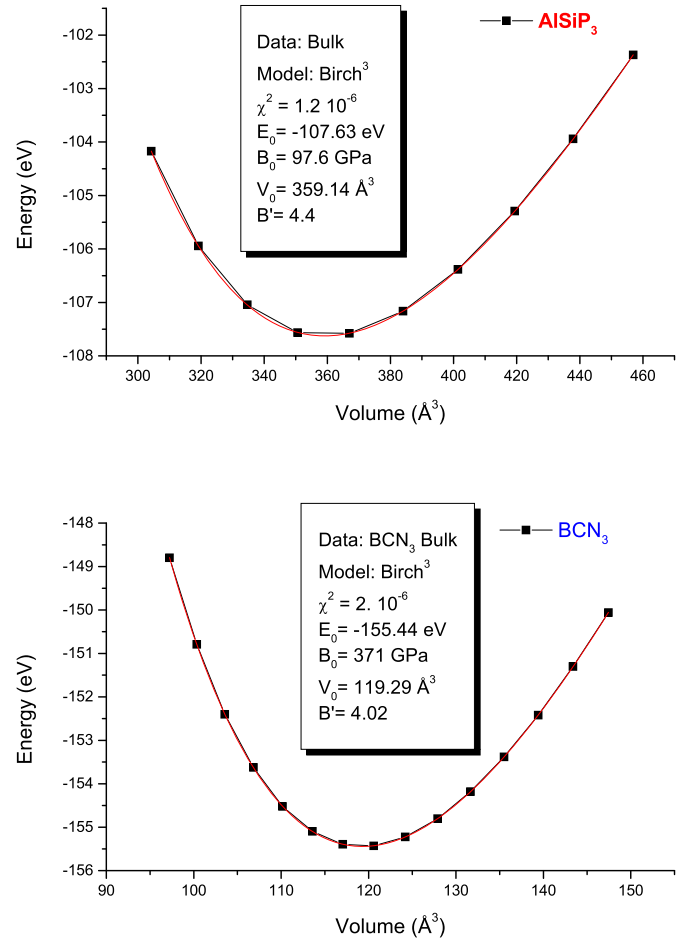


Fig. 3. Energy volume ( $E,V$ ) curves of  $\text{AlSiP}_3$  and  $\text{BCN}_3$  and Birch equation of state EOS fit values shown in the insert (see text).  $\chi^2$  designates the goodness of fit.

$$B(V) = -V \cdot \frac{dP}{dV} = V \cdot \frac{d^2E}{dV^2},$$

where  $V$  is the volume of the unit cell,  $E(V)$  is the energy per unit cell at volume  $V$ , and  $P(V)$  is the pressure required to keep the unit cell at volume  $V$ . Since the calculations can only provide a restricted set of energies  $E(V_i)$ , the second derivative must be approximated. The least squares fit of the curves  $E$  vs.  $V$  has been done using the Birch equation of state EOS up to the 3rd order [24]:

$$E(V) = E_0 + \frac{9}{8} B_0 V_0 \left[ \left( \frac{V_0}{V} \right)^{\frac{2}{3}} - 1 \right]^2 + \frac{9}{16} B_0 (B'_0 - 4) V_0 \left[ \left( \frac{V_0}{V} \right)^{\frac{2}{3}} - 1 \right]^3,$$

where  $E_0$ ,  $V_0$ ,  $B_0$ ,  $B'_0$  and are respectively the energy and the volume at equilibrium, the bulk modulus and its pressure derivative. The bulk modulus can then be obtained by analytic differentiation of above equation. The obtained values are given in the inserts of Fig. 3 showing the energy-volume curves. The fit curves reproduce the trends of the geometry optimization for the volume with a small deviation.

The interesting result is in the magnitude of the bulk modulus of  $B_0 = 97$  GPa for  $\text{AlSiP}_3$  and the more than 3 times higher value of

$B_0 = 371$  GPa for  $\text{BCN}_3$ , thus placing the latter in the range of very hard materials [8]; whereas the former compound is in the range of soft compounds as the intermetallic ones [25].

### 3.3. Elastic properties and mechanical stability

In view of the peculiar result of high hardness obtained for  $\text{BCN}_3$ , it was relevant to check it with the calculation of the set of elastic constants and to derive its mechanical properties stability from their combination.

The elastic properties are determined by performing finite distortions of the lattice and deriving the elastic constants from the strain-stress relationships. In orthorhombic symmetry there are nine independent elastic stiffness constants  $C_{11}$ ,  $C_{12}$ ,  $C_{13}$ ,  $C_{23}$ ,  $C_{22}$ ,  $C_{33}$ ,  $C_{44}$ ,  $C_{55}$  and  $C_{66}$ . Most encountered compounds are polycrystalline where monocrystalline grains are randomly oriented so that on a large scale, such materials can be considered as statistically isotropic. They are then completely described by the bulk modulus  $B$  and the shear modulus  $G$ , which may be obtained by averaging the single-crystal elastic constants. The most widely used averaging method of the elastic stiffness constants is Voigt's one [26] based on a uniform strain. The calculated set of elastic constants in  $\text{BCN}_3$  in units of GPa are:

$C_{11} = 1024$ ;  $C_{12} = 188$ ;  $C_{13} = 93$ ,  $C_{23} = 264$ ,  $C_{22} = 1004$ ,  $C_{33} = 341$ ,  $C_{44} = 370$ ,  $C_{55} = 400$  and  $C_{66} = 337$ .

It is interesting to note that  $C_{11}$  magnitude is close to that of diamond ( $C_{11} = 1050$  GPa) which is characterized by three independent elastic constants in its cubic form:  $C_{44} = 600$  GPa and  $C_{12} = 137$  GPa [8]. Note that elastic constant  $C_{11}$  represents elasticity in length.

All  $C_{ij}$  values are positive and their combinations:  $C_{11} > C_{12}$ ,  $C_{11}C_{33} > C_{13}^2$  and  $(C_{11} + C_{12})C_{33} > 2C_{13}^2$  obey the rules pertaining to the mechanical stability of the compound. The bulk ( $B_V$ ) and shear ( $G_V$ ) modules following Voigt are formulated as:

$$B_V = 1/9\{C_{11} + C_{22} + C_{33} + 2(C_{12} + C_{23} + C_{31})\} \text{ and}$$

$$G_V = 1/15\{C_{11} + C_{22} + C_{33} - (C_{12} + C_{23} + C_{31}) - 3(C_{44} + C_{55} + C_{66})\}$$

[27].

The numerical values are then:  $B_V = 384$  GPa and  $G_V = 326$  GPa. The value of  $B_V$  is larger but still in fair agreement with the one obtained from the EOS fit (Fig. 3, inserts) thus validating the two different approaches. The shear modulus which defines the rigidity of the material is also of large magnitude. In this context the Pugh's  $G/B$  ratio [28] which is an indicator of brittleness or ductility for  $G/B > 0.5$  and  $G/B < 0.5$ , respectively is obtained for  $\text{BCN}_3$  as  $G/B = 0.85$ , indicating brittleness, contrary to the coinage metals Ag, Pt, or Au with  $G/B$  ratios in the range of 0.4–0.2 [29].

### 3.4. Vibrational frequencies

The vibration frequencies are obtained from the calculated Hessian matrix (second derivative with respect to energy  $\delta^2 E / \delta r^2$ ) based on finite differences, by moving each atom about its Cartesian position. The frequencies are calculated at  $\Gamma$  zone center. The computational effort is important especially in the present case where 20 atoms are involved. Also with a huge supercell  $2a \times 2b \times 2c$  similar results could only be obtained by decreasing the BZ k integration.

In a non linear molecule there are  $3n - 6$  degrees of freedom ( $n =$  number of atoms) which then amount to 54 in  $\text{BCN}_3$ . The frequencies in Tera-Hz and in  $\text{cm}^{-1}$  are displayed in Table S1

(supplementary material). They correspond to symmetrical and antisymmetrical stretching, wagging, twisting, scissoring, breathing modes. The video provided in supplementary material allows the reader to follow along with Table S1 the evolution from rigid lattice modes (along the three axes) at very low frequencies up to C-N stretching and twisting at high frequencies. All 54 frequencies are positive and define a stable system.

Supplementary data related to this article can be found at <http://dx.doi.org/10.1016/j.cocom.2016.03.003>.

## 4. Electron localization function ELF mapping

The bonding peculiarities following the arrangement of pyrite-wurtzite motifs in Fig. 2 can be further illustrated by the electron localization function (ELF) mapping which is a real space analysis [30,31]. ELF is a normalized function:  $0 \leq \text{ELF} \leq 1$  with zero

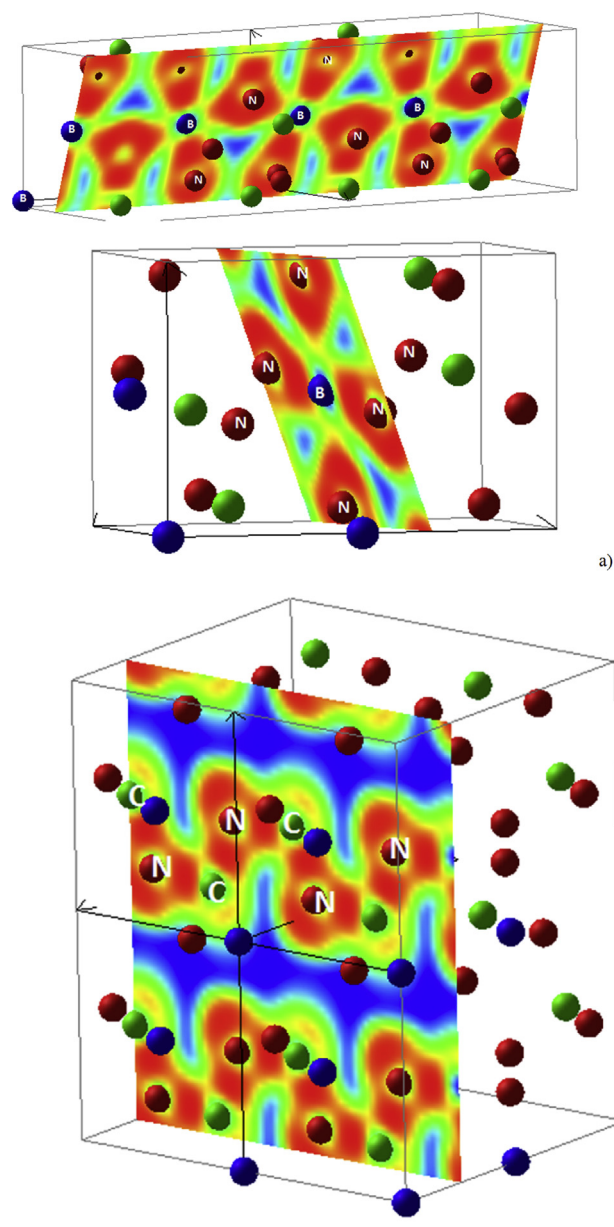


Fig. 4.  $\text{BCN}_3$ . a) ELF slices crossing basal planes of  $\text{BN}_6$ -like octahedra along two directions and b) plane crossing an array of  $\text{CN}_4$ -like tetrahedra over four adjacent cells.

localization  $ELF = 0$  (blue areas in the plots), strong localization for 1 (red areas) and free electron like behavior for  $ELF = 1/2$  (green areas). The selected planes are shown in Fig. 4. This follows from the structure sketch of Fig. 2 (as well as the structure in the video provided in supplementary matter). The nitride-like anionic substructure is clearly observed from the strong red areas around nitrogen whereas B and C sites are embedded in green-like areas because of the bonding with the anions. Opposite behaviors characterize the *pyrite* versus the *wurtzite*-like surrounding of B and C respectively: while there is continuity of electron localization in the centrosymmetric *pyrite*-like entities, blue areas of no localization are present between the rows of non centrosymmetric tetrahedra as shown in Fig. 4b.

## 5. Electronic band structure and density of states

Using the calculated structural data in Table 1 we analyzed the electronic band structure. We note here that only comparative aspects are to be taken as relevant, i.e. we do not pretend providing absolute band gaps for instance.

Fig. 5 shows the band dispersions along the major directions of the orthorhombic Brillouin zone. Both  $AlSiP_3$  and  $BCN_3$  are

characterized by insulating behavior in so far that the zero energy along the  $y$ -axis is with respect to the top of the valence band (VB) at  $E_V$  separated by an energy gap from the empty conduction band (CB). This is also followed in Fig. 6 showing the DOS. However  $AlSiP_3$  is an indirect gap (between  $\Gamma_{\text{Valence}}$  and  $T_{\text{Conduction}}$ ) semiconductor with a very small magnitude of  $\sim 0.05$  eV whereas  $BCN_3$  is revealed as an insulator with a direct gap,  $\Gamma_V - \Gamma_C = \sim 4$  eV. Testing local density approximation LDA [32] potentials led to similar trends but with smaller gap magnitudes due to the overbinding character of the LDA.

The other major difference is in the larger extension of the VB in  $BCN_3$  due to the larger electronegativities of the lighter elements constituents, especially N and P:  $\chi(N) \sim 3.04$  versus  $\chi(P) \sim 2.19$ . Lastly there is a separation between the lower part of VB ( $-15$ ,  $-9$  eV) with respect to the upper part extending up to  $E_V$  in  $AlSiP_3$ , not observed in  $BCN_3$  which presents a rather continuous shape. This is likely to arise from the shorter interatomic distances in the latter leading to stronger covalent like interactions in the B-C-N based compound.

These observations are detailed further with the site projected densities of states (PDOS) in Fig. 6. The common VB features are

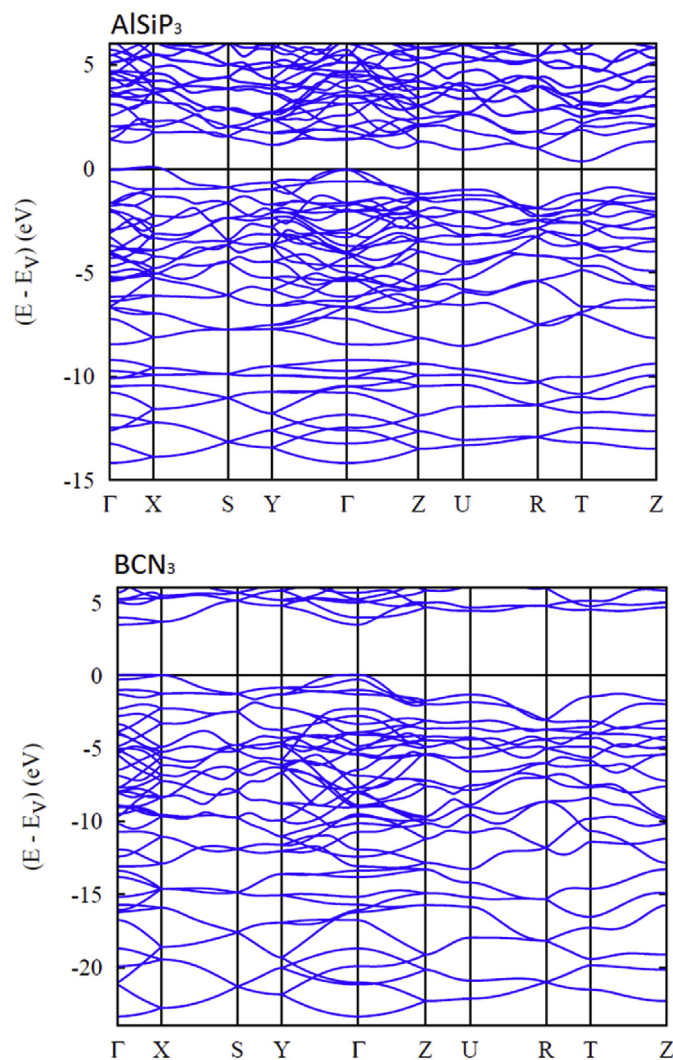


Fig. 5.  $AlSiP_3$  and  $BCN_3$ . Electronic band structures along major directions of the simple orthorhombic Brillouin zone.

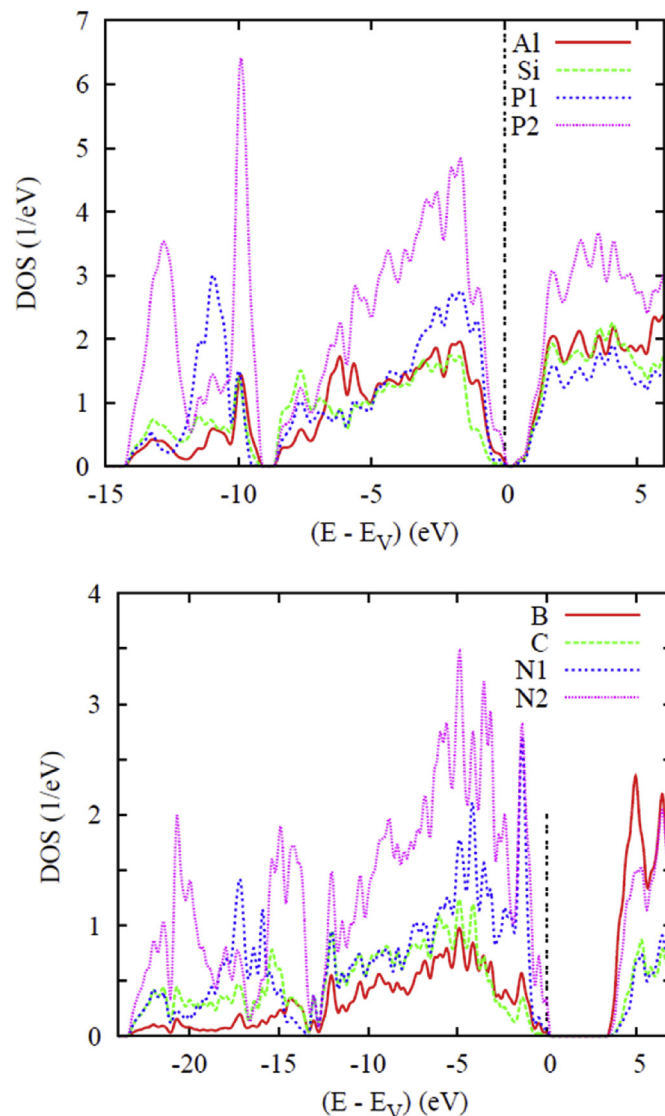


Fig. 6.  $AlSiP_3$  (top) and  $BCN_3$  (bottom): Site projected electronic density of states PDOS.

related with the larger intensities of the P and N anions PDOS versus the Al, Si and B, C ones, stressing further their respective behaviors as anions and cations. Also the DOS intensities are almost twice larger in AlSiP<sub>3</sub> due to the larger number of electrons of such 2nd period elements versus 1st period B, C and N. The top of VB is dominated by anionic PDOS although cationic PDOS are also present. The quantum mixing (hybridization) between the valence states of the constituents is signaled by the similar PDOS shapes as for B with N<sub>2</sub> and C with N<sub>1</sub>. The bottom of the CB is a mixture of B and N<sub>2</sub> states in BCN<sub>3</sub>, a feature less obvious in AlSiP<sub>3</sub>

## 6. Proposed synthesis routes

In view of the favorable computational results concerning the stability of the new ternary compound, synthesis routes are being considered.

The high nitrogen content of BCN<sub>3</sub> lets propose synthesis routes based on highly nitriding conditions. Classical protocols of solid state chemistry calling for high temperatures and pressures such as achieved by using anvil pressure cells can be investigated.

Alternatively we are exploring, in particular mild temperature conditions with mechano-synthesis by energetic grinding of the reactants (C, BN ...) together with high nitrogen content hydrazine (N<sub>2</sub>H<sub>4</sub>) under controlled inert ultra pure N<sub>2</sub> atmosphere.

## 7. Conclusions and prospective works

In this work we have proposed from DFT calculations of geometry optimizations and energy related quantities, a novel hard material candidate, orthorhombic BCN<sub>3</sub>. This light elements based ternary can be visualized as the intergrowth of tetrahedral *wurtzite* *w*-CN<sup>+</sup> and *pyrite* *py*-BN<sub>2</sub><sup>-</sup> entities. The compound can be considered as a nitride-dinitride chemical system related with Zintl phases. Significantly short interatomic distances:  $d(\text{C-N}) = 1.47 \text{ \AA}$  and  $d(\text{N-N}) = 1.43 \text{ \AA}$  result into high magnitude bulk modulus of  $B_0 = 371 \text{ GPa}$  obtained from E,V equation of state (EOS). The set of elastic constants  $C_{ij}$  are in accordance with the mechanical stability and provide a shear to bulk modulus ratio  $G/B = 0.85$  pertaining to a brittle material. The  $\Gamma$ -zone vibrational modes are all positive definite and illustrated in an attached video animation (supplementary material). Different synthesis protocols are being investigated.

## Acknowledgements

We thank the Doctoral school of Science and Technology of the

Lebanese University for financial help. Supports from the CNRS-France, the INC-CNRS-France and the *Conseil Régional d'Aquitaine* are gratefully acknowledged.

## Appendix A. Supplementary data

Supplementary data related to this article can be found at <http://dx.doi.org/10.1016/j.cocom.2016.03.003>.

## References

- [1] R.M. Hazen, *The Diamond Makers*, Cambridge University Press, 1999, pp. 100–113. ISBN 0-521-65474-2.
- [2] F.P. Bundy, R.H. Wentorf Jr., *J. Chem. Phys.* 38 (1963) 1144.
- [3] D.M. Teter, R.J. Hemley, *Science* 271 (1996) 53.
- [4] A.Y. Liu, M.L. Cohen, *Science* 245 (1989) 841.
- [5] M. Mattesini, S.F. Matar, *Phys. Rev. B* 65 (2002) 7511010–7511014.
- [6] P. Hohenberg, W. Kohn, *Phys. Rev.* 136 (1964). B864 & W. Kohn, L. J. Sham, *Phys. Rev.* 140 (1965) A1133.
- [7] F. Thévenot, *J. Eur. Ceram. Soc.* 6 (1990) 205.
- [8] M. Mattesini, S.F. Matar, *Intl. J. Inorg. Mater.* 3 (2001), 943 and *Comp. Mater. Sci.* 20 (2001) 107.
- [9] V.L. Solozhenko, D. Andrault, G. Fiquet, M. Mezouar, D.C. Rubie, *Appl. Phys. Lett.* 78 (2001) 1385.
- [10] J.L. He, L.C. Guo, E. Wu, X.G. Luo, Y.J. Tian, *J. Phys. Condens. Matter* 46 (2004) 32.
- [11] J. Hao, H. Liu, W. Lei, X. Tang, J. Lu, D. Liu, Y. Li., *J. Phys. Chem. C* 119 (2015) 28614.
- [12] H. G. v. Schnering, G. Menge, *J. Solid State Chem.* 28 (1979) 13.
- [13] T. K. Chattopadhyay, H.G. v Schnering, *Z. Kristallogr.*, 1984, 167, 1.
- [14] G. Kresse, J. Furthmüller, *Phys. Rev. B* 54 (1996) 11169.
- [15] G. Kresse, J. Joubert, *Phys. Rev. B* 59 (1999) 1758.
- [16] P.E. Blöchl, *Phys. Rev. B* 50 (1994) 17953.
- [17] J. Perdew, K. Burke, M. Ernzerhof, *Phys. Rev. Lett.* 77 (1996) 3865.
- [18] W.H. Press, B.P. Flannery, S.A. Teukolsky, W.T. Vetterling, *Numerical Recipes*, Cambridge University Press, New York (, 1986.
- [19] P.E. Blöchl, *Phys. Rev. B* 49 (1994) 16223.
- [20] M. Methfessel, A.T. Paxton, *Phys. Rev. B* 40 (1989) 3616.
- [21] H.J. Monkhorst, J.D. Pack, *Phys. Rev. B* 13 (1976) 5188.
- [22] S.F. Matar, R. Pöttgen, *Z. Naturf. B*, 68b (2013) 23.
- [23] H. Schaffer, B. Eisenmann, W. Mueller, *Angew. Chem.* 85 (1973) 742.
- [24] F. Birch, *J. Geophys. Res.* 83 (1978) 1257.
- [25] S.F. Matar, B. Chevalier, R. Pöttgen, *Intermetallics* 31 (2012) 88.
- [26] S.F. Matar, in: T. I (Ed.), *Matériaux ultra-durs: Concepts et Modélisations. Série Techniques de l'ingénieur*, 6630, Sciences et Techniques, Paris. - AF, 2009, p. 20.
- [27] P.T. Jochym, K. Parlinski, P. Krzywiec, *Comp. Mater. Sci.* 29 (2004) 414.
- [28] S.F. Pugh, *Phil. Mag.* 45 (1954) 823.
- [29] S. Kamran, K. Chen, L. Chen, L. Zhao, *J. Phys. Condens. Matter* 20 (2008) 085221.
- [30] A.D. Becke, K.E. Edgecombe, *J. Chem. Phys.* 92 (1990) 5397.
- [31] B. Silvi, A. Savin, *Nature* 371 (1994) 683.
- [32] D.M. Ceperley, B.J. Alder, *Phys. Rev. Lett.* 45 (1980) 566.